A STRUCTURE TENSOR BASED VORONOI DECOMPOSITION TECHNIQUE FOR OPTIC CUP SEGMENTATION

P. Kevin Raj[2], J. R. Harish Kumar[1,2], Subramanya Jois[1], Harsha S.[1] and Chandra Sekhar Seelamantula[1]

[1]Department of Electrical Engineering, Indian Institute of Science, Bangalore, India
[2]Department of E and E Engineering, Manipal Institute of Technology, MAHE, Manipal, India
kevinyitshak@gmail.com, {harishj, subramanyaj, harshasridha, chandrasekhar}@iisc.ac.in

ABSTRACT

We present a technique for segmentation of optic cup based on the structural features found in blood vessels surrounding the optic cup region. The advantage of using such features is that they are robust to variations in the properties of the fundus image such as brightness, contrast, etc. The main features used in the technique are vessel bends (also called as *landmark points* or *kinks*), which are identified by applying the Harris corner detection algorithm on the optic disc region, followed by a *Voronoi* image decomposition. Pratt's circle fitting algorithm is employed on the extracted landmark points to segment the optic cup region. The proposed technique is validated on a total of 191 images taken from publicly available fundus image datasets, namely, Drishti-GS and MESSIDOR. Performance metrics such as sensitivity, specificity, accuracy, Jaccard's index, and Dice coefficient are computed to be 85%, 97%, 96%, 69.5%, and 81%, respectively, which indicates that the proposed technique for optic cup segmentation is competitive with the state-of-the-art methods.

Index Terms— Optic cup segmentation, vessel bends, Harris corner detection, Voronoi decomposition, circle fit.

1. INTRODUCTION

Optic cup (OC) is the term given for a region of inactive neuronal clusters within the optic nerve head in the retina. It is perceived as a region with a bright pallor within the optic disc (OD) region in retinal fundus images. Given that various factors affect the quality of the captured fundus image, the pallor is not always distinct. In such cases, the detection of the OC region using conventional methods that rely on pallor for segmentation might be erroneous. Hence, there is a need for a technique to segment the OC region that relies on structural features that are independent of the contrast or texture of the captured fundus image. Due to increase in intra-ocular pressure, the vessels inside the optic nerve head deform resulting in the formation of '*kinks*' (vessel bends) [1]. In this paper, we propose a technique that exploits these kinks as structural features to determine the contours of the OC region. Fig. 1 shows a fundus image and the optic cup outline obtained using the proposed technique.

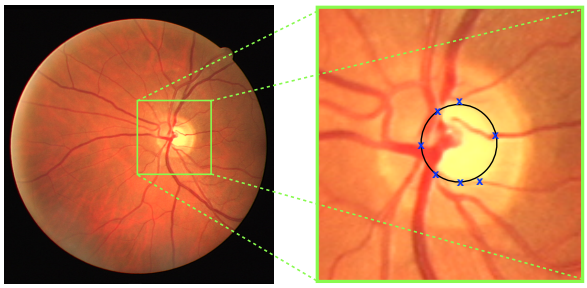

Fig. 1: [Color online] Left: Fundus image; Right: Optic cup segmentation by the proposed technique that uses vessel bends as features.

1.1. Prior Work

Optic cup segmentation is a widely addressed problem and several solutions have been suggested. Significant advancements have been made over the past few years both on the conventional image processing and deep learning fronts. For a comprehensive study on classical image processing based OC and OD segmentation techniques, the reader is referred to the survey carried out by Almazroa et al. [2]. More recently, Harish et al. presented a comprehensive study wherein they highlighted the differences in the different grading metrics for glaucoma and proposed a novel methodology for computation of the rim-to-disc-ratio [3]. In their work, they utilize an active disc based segmentation model for segmentation of OD and OC which is competitive with most existing approaches. On the neural networks front, Xu et al. [4] proposed superpixel classification technique formulated as a low-rank representation to classify OC from fundus image. Chakravarty et al. [5] used a depth-based supervised method with a coupled

The authors would like to thank Dr. Yogish S Kamath and Dr. Rajani Jampala from Kasturba Medical College (KMC), MAHE, Manipal, India for providing manual annotations of the optic cup region. This work was supported by the Ministry of Human Resource Development under the IMPRINT India Initiative (Domain: Healthcare; Project No.: 6013).

Authorized licensed use limited to: Max-Planck-Institut fuer Informatik . Downloaded on November 15,2023 at 12:54:36 UTC from IEEE Xplore. Restrictions apply.

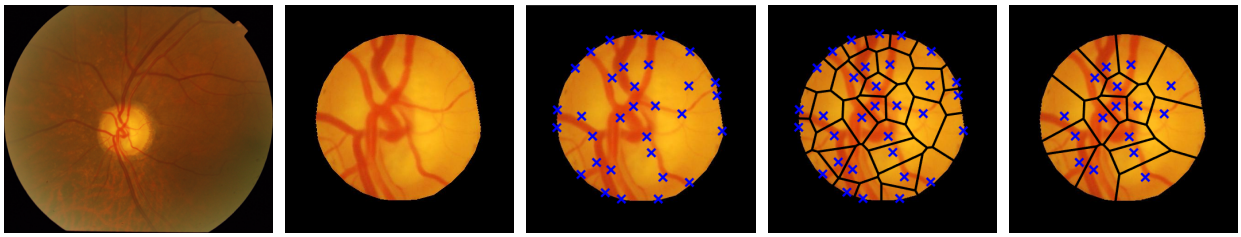

(a) (b) (c) (d) (e)

Fig. 2: [Color online] (a) Fundus image; (b) Segmented optic disc region; (c) landmark points obtained using the multiscale Harris corner detector; Voronoi decomposition using (d) the initial landmark points; and (e) after removing the landmark points on the OD boundary.

sparse dictionary for OC segmentation. Zilly et al. [6] proposed an entropy sampling based boosting of convolutional filters and ensemble learning approach for segmenting OC. Sevastopolsky et al. [7] employed a modified U-net convolution architecture for OC segmentation. Recently, Edupuganti et al. [8] used a fully convolution neural network to perform segmentation of the OC region. Yin et al. [9] suggested a novel statistical model based method for segmenting the OC. Xu et al. [10] proposed a method using deformable snakes for delineating the OC region. Joshi et al. [11–13] were amongst the first to contribute a series of methods for OD and OC segmentation using kinks. Accurate differentiation of relevant kinks from the irrelevant ones remains a difficult problem. In the following sections, we discuss a new technique addressing the detection of the relevant kinks or landmark points for accurate segmentation of the OC region.

Contribution of this paper: The key novelty of this paper is the use of Voronoi decomposition based selection of relevant kinks (landmark points) obtained from a multiscale Harris corner detector for determining the OC boundary.

2. PROPOSED METHOD

We propose a structure tensor based Voronoi decomposition technique for accurate segmentation of the OC. The regions corresponding to the vessel bends within the OD region were found to be desirable for OC segmentation. We use expert annotations to isolate the OD region, followed by: (i) determination of landmark points within the OD region [14] using structure tensor based multiscale Harris corner detection; and (ii) application of the Voronoi decomposition [15] on the points obtained in Step (i) to get relevant landmark points as illustrated in Fig. 2. Below, we expand upon the aforementioned stages.

2.1. Structure Tensor Based Harris Corner Detection

Consider an image represented by the function $I(x, y)$, whose horizontal and vertical derivatives are $\partial_x I$ and $\partial_y I$, respectively:

$$\begin{aligned} \partial_x I &= I(x,y) * g^{(1)}_{\sigma_d}(x,y), \\ \partial_y I &= I(x,y) * g^{(2)}_{\sigma_d}(x,y), \end{aligned} \tag{1}$$

where $*$ denotes the convolution operation, and $g^{(1)}_{\sigma_d}$ and $g^{(2)}_{\sigma_d}$ are the spatial derivative operators along x and y, respectively, having standard deviation σ_d. The structure tensor S_T at each point is calculated by computing the outer product of the gradient vector with itself as given below:

$$S_T = \begin{bmatrix} v * (\partial_x I)^2 & v * (\partial_x I \partial_y I) \\ v * (\partial_y I \partial_x I) & v * (\partial_y I)^2 \end{bmatrix}, \tag{2}$$

where v is a gaussian filter with standard deviation $\sigma_a = 0.7\,\sigma_d$. The detection of landmark points $L_p(x, y)$ is performed using Harris corner detection algorithm [14] on the green channel of the fundus image, which gives the best contrast of blood vessels (darker blood vessels on a bright background). The likelihood of a point being detected as a corner is determined using:

$$R_p(x, y) = \det(S_T) - k\ \mathrm{trace}^2(S_T). \tag{3}$$

where k is the trade-off factor and is typically set to 0.04. In a multiscale framework, the set of landmark points L_p (shown in Fig. 2(c)) is determined using (1), (2) & (3) for standard deviation ${\sigma_d}^i = \alpha^{i-1}\,\beta$; where, $i = 1$ to 5, α is the step size, and β is the scale factor.

2.2. Voronoi decomposition

We partition the region of interest in the fundus image into convex regions based on the Euclidean distance between the landmark points such that each region contains exactly one landmark point [15]. The points detected at the center of OC and border of OD, due to the primary blood vessels and OD mask, respectively are redundant as they do not correspond to the OC boundary. These points are separated into corresponding sub-regions called Voronoi cells (VC) as follows.

Consider a set S of co-planar points P_n with $n \geq 3$, $S = \{P_1, P_2, \cdots, P_n\}$, where $P_i = (p_i, p_j)$. The Euclidean distance between P_i and a point $x = (x_1, x_2)$ is given by

$$D(P_i, x) = \sqrt{(p_i - x_1)^2 + (p_j - x_2)^2},$$

Authorized licensed use limited to: Max-Planck-Institut fuer Informatik . Downloaded on November 15,2023 at 12:54:36 UTC from IEEE Xplore. Restrictions apply.

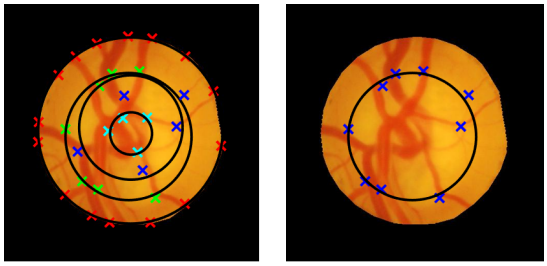

(a) (b)

Fig. 3: [Color online] (a) Different levels of landmark points; red: 1^{st} level, green: 2^{nd} level, blue: 3^{rd} level, cyan: 4^{th} level, and their corresponding circle fits; (b) The final segmented OC region using the proposed method.

The perpendicular bisector of the line joining the points P_1 and P_2 is given by

$$B(P_1, P_2) = \{x | D(P_1, x) = D(P_2, x)\},$$

Let $H(P_1, P_2)$ denote the half-plane containing the set of all points that are closer to P_1 than to P_2:

$$H(P_1, P_2) = \{x | D(P_1, x) < D(P_2, x)\},$$

The Voronoi cell containing P_1 is the intersection of several such half-planes and is specified as

$$VC(P_1, S) = \bigcap_{P_i \in S, i \neq 1} H(P_1, P_i), \quad (4)$$

The Voronoi decomposition is the union of the closure of the Voronoi cells:

$$V(S) = \bigcup_{P_i, P_j \in S, i \neq j} \overline{VC(P_1, S)} \cap \overline{VC(P_2, S)}. \quad (5)$$

where the overbar denotes set closure.

Let V_e be the vertices of the Voronoi decomposition, which are the endpoints of $(V(S))$ that belong to the common boundary of three or more Voronoi cells. A Voronoi cell is bounded if the number of vertices (V_e) is greater than or equal to three. Fig. 2(d) shows that the outer most Voronoi cells contributed by landmark points on the OD boundary (labeled as 1^{st} level points) are not bounded and discarded from further analysis. We again perform Voronoi decomposition on the new set of points obtained after removing the outer most points (cf. Fig. 2(e)). The set of points that lie in unbounded Voronoi cells are labelled as the 2^{nd} level points. The 3^{rd} and 4^{th} level points are obtained in a similar fashion. Selection of points that constitute the relevant kinks from the identified ones is based on the intensity and the area of the pallor. We consider the brightest pixel group B_p within the OD obtained from a 4-level Otsu thresholding. If B_p constitutes to more than 50% of the OD area, then we consider 2^{nd} level points as the relevant kinks, else the 4^{th} level points are considered as the relevant ones. In most cases, we have observed that the 2^{nd} level points are reliable for determining the OC boundary. The procedure for removing irrelevant landmark points is summarized in Algorithm 1. Finally, a circle is fit to the relevant landmark points using Pratt's technique [22] resulting in an accurate OC segmentation as shown in Fig. 3(b).

Algorithm 1: Procedure for selection of relevant landmark points using Voronoi decomposition

```
for i= 1: 4
apply Voronoi decomposition on set of points L_p
if no. of vertices V_e ≥ 3 then
    mark cells as bounded; retain points in L_p
else
    mark cells as unbounded; discard points from L_p
    store discarded points in L_p'(i)
end
end for
determination of relevant points from L_p'
if area (B_p) > area (50 % of OD) then
    OC defined by L_p'(2) [2nd level points]
else
    OC defined by L_p'(4) [4th level points]
end
end algorithm
```

3. EXPERIMENTAL RESULTS

The proposed methodology has been validated on images taken from the publicly available Drishti-GS [23] and MESSIDOR [24] datasets with 101 and 90 images, respectively, selected from them. The selection has been done to maintain diversity with regards to contrast and texture of the images. Some results from the segmentation of the OC region and the subsequent circle fitting are illustrated in Fig. 4. As can be observed, the match between the expert annotations and the algorithm generated one is significant. Table 1 provides a quantitative measure of the performance using the Jaccard index (J_i) and Dice coefficient (D_c) employed as the metrics. A performance comparison indicates that the proposed model is competitive with the state-of-the-art methods. Table 2 gives a summary of the performance of the algorithm using standard performance metrics. The high sensitivity, specificity and accuracy scores reflect the capability of the algorithm to accurately determine the relevant kinks in the vessels to be used for mapping the contour of the OC region. From the scores, it can be inferred that the overall performance of the algorithm marks it as a capable solution for handling the challenge faced by many approaches for demarcation of the OC in retinal fundus images.

Authorized licensed use limited to: Max-Planck-Institut fuer Informatik . Downloaded on November 15,2023 at 12:54:36 UTC from IEEE Xplore. Restrictions apply.

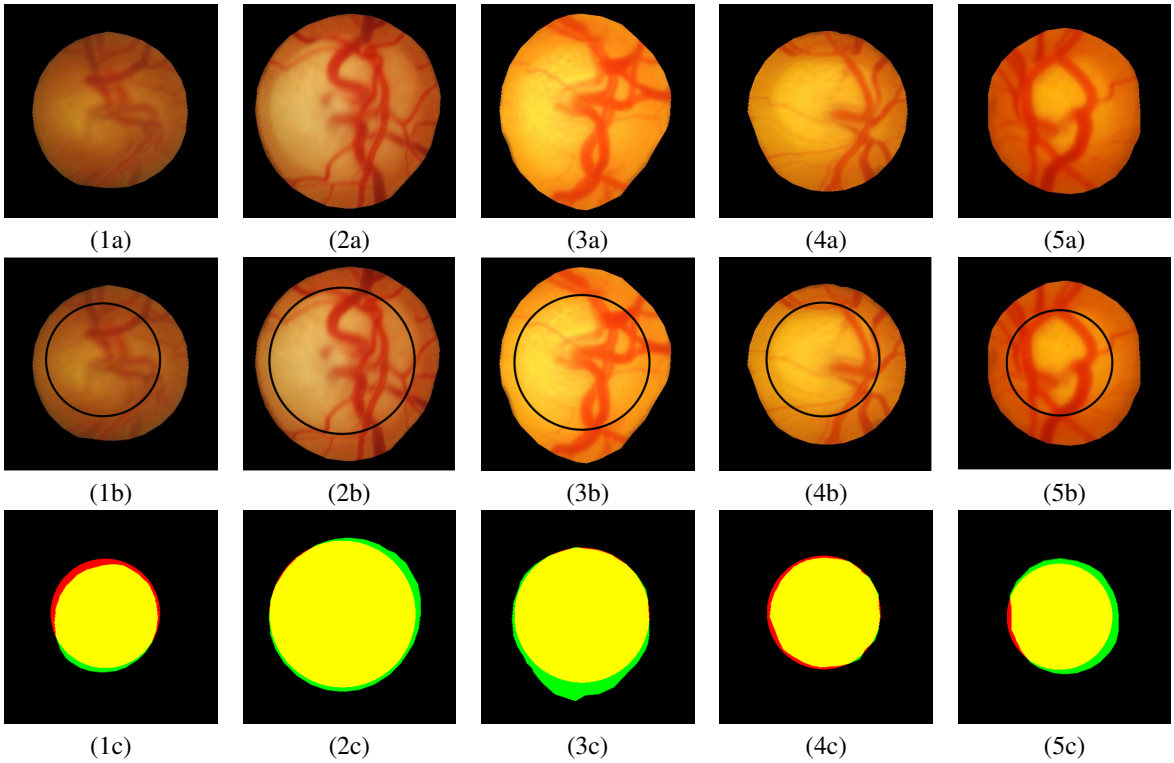

Fig. 4: [Colour online] (1a-5a): Segmented optic disc region, (1b-5b): Optic cup segmentation using the proposed technique, (1c-5c): Comparison of the algorithm output (shown in red) vis-à-vis the expert annotations (shown in green); the region shown in yellow indicates overlap.

Table 1: Performance comparison of the proposed method with the state-of-the-art techniques.

Algorithm	**Dataset used** (# of Images)	J_i	D_c
Yin et al. [9]	Local (325)	0.68	0.81
Joshi et al. [12]	Drishti-GS (101)	0.63	0.77
Chakravarthy et al. [5]	Drishti-GS (101)	0.67	0.80
Cheng et al. [16]	SiMES (650)	0.61	0.75
Xu et al. [4]	Origa (650)	0.74	0.85
Yin et al. [17]	Origa (650)	0.79	0.83
Pardha et al. [18]	Local (59)	0.80	0.89
Harish et al. [19]	Drishti-GS (101)	0.57	0.73
Joshi et al. [11]	Aravind Eye Hospital (138)	0.72	0.84
Liu et al. [20]	SERI (140)	0.50	0.67
Zilly et al. (ML) [6]	Drishti-GS (10)	0.77	0.87
Sevastopolsky (ML) [7]	Drishti-GS (50)	0.74	0.85
BCF (ML) [21]	Drishti-GS (10)	0.71	0.83
Proposed method	Drishti-GS (101)	0.70	0.82
	MESSIDOR (90)	0.69	0.80

Table 2: Performance of the proposed OC segmentation algorithm; S_e - sensitivity; S_p - specificity; Acc - accuracy; J_i - Jaccard index and D_c - Dice coefficient.

Database (# of images)	S_e	S_p	Acc	J_i	D_c
Drishti-GS (101)	0.87	0.95	0.93	0.7	0.82
MESSIDOR (90)	0.83	0.99	0.99	0.69	0.80
Average (191)	0.85	0.97	0.96	0.695	0.81

4. CONCLUSIONS

In this paper, we presented a novel technique for automated segmentation of the OC region in retinal fundus images. The novelty of the solution is that unlike conventional techniques that approach the problem keeping pallor of the OC region in mind, the proposed technique relies on structural properties – namely, the kinks found in retinal vasculature to determine the contour of the OC. Through this approach, the model overcomes one of the biggest hurdles in OC segmentation, namely, widely varying contrast in fundus images, thereby ensuring greater ease in assessment of retinal pathologies such as glaucoma that are dependent on the extraction of the OC contour. The method has been validated on the publicly available Drishti-GS and MESSIDOR datasets and has been shown to be on par with the conventional approaches. The segmentation of the OC could be further improved through combined mapping of the said region using contrast and kinks.

Authorized licensed use limited to: Max-Planck-Institut fuer Informatik . Downloaded on November 15,2023 at 12:54:36 UTC from IEEE Xplore. Restrictions apply.

5. REFERENCES

[1] J. A. Giaconi et al., *Pearls of Glaucoma Management*, Springer, USA, 2010.

[2] A. Almazroa et al., "Optic disc and optic cup segmentation methodologies for glaucoma image detection: A survey," *Journal of Ophthalmology*, 2015.

[3] J. R. Harish Kumar et al., "Rim-to-disc ratio outperforms cup-to-disc ratio for glaucoma prescreening," *Scientific reports*, vol. 9, no. 1, pp. 7099, 2019.

[4] Y. Xu et al., "Optic cup segmentation for glaucoma detection using low-rank superpixel representation," in *Proceedings of International Conference on Medical Image Computing and Computer Assisted Intervention (MICCAI)*, 2014, pp. 788–795.

[5] A. Chakravarty and J. Sivaswamy, "Coupled sparse dictionary for depth-based cup segmentation from single color fundus image," in *Proceedings of International Conference on Medical Image Computing and Computer Assisted Intervention*, 2014, pp. 747–754.

[6] J. G. Zilly et al., "Glaucoma detection using entropy sampling and ensemble learning for automatic optic cup and disc segmentation," in *Computerized Medical Imaging and Graphics*, 2017, vol. 55, pp. 28–41.

[7] A. Sevastopolsky, "Optic disc and cup segmentation methods for glaucoma detection with modification of u-net convolutional neural network," *Pattern Recognition and Image Analysis*, vol. 27, no. 3, pp. 618–624, 2017.

[8] V. G. Edupuganti et al., "Automatic optic disk and cup segmentation of fundus images using deep learning," in *Proceedings of IEEE International Conference on Image Processing (ICIP)*, 2018, pp. 2227–2231.

[9] F. Yin et al., "Automated segmentation of optic disc and optic cup in fundus images for glaucoma diagnosis," in *Proceedings of IEEE International Symposium on Computer-Based Medical Systems*, 2012, pp. 1–6.

[10] Xu et al., "Optic disk feature extraction via modified deformable model technique for glaucoma analysis," *Pattern Recognition*, vol. 40, no. 7, pp. 2063–2076, 2007.

[11] G. D. Joshi et al., "Optic disk and cup segmentation from monocular color retinal images for glaucoma assessment," *IEEE Transactions on Medical Imaging*, vol. 30, no. 6, pp. 1192–1205, 2011.

[12] G. D. Joshi et al., "Depth discontinuity-based cup segmentation from multiview color retinal images," *IEEE Transactions on Biomedical Engineering*, vol. 59, no. 6, pp. 1523–1531, 2012.

[13] G. D. Joshi and J. Sivaswamy, "Vessel bend-based cup segmentation in retinal images," in *Proceedings of IEEE International Conference on Pattern Recognition*, 2010, pp. 2536–2539.

[14] C. Harris and M. Stephens, "A combined corner and edge detector.," *Proceedings of Alvey Vision Conference*, vol. 15, no. 50, pp. 10–60, 1988.

[15] C. B. Barber et al., "The quickhull algorithm for convex hulls," *ACM Transactions on Mathematical Software (TOMS)*, vol. 22, no. 4, pp. 469–483, 1996.

[16] J. Cheng et al., "Superpixel classification based optic disc and optic cup segmentation for glaucoma screening," *IEEE Transactions on Medical Imaging*, vol. 32, no. 6, pp. 1019–1032, 2013.

[17] F. Yin et al., "Sector-based optic cup segmentation with intensity and blood vessel priors," in *Proceedings of IEEE International Conference on Engineering in Medicine and Biology Society*, 2012, pp. 1454–1457.

[18] P. S. Mittapalli and G. B. Kande, "Segmentation of optic disk and optic cup from digital fundus images for the assessment of glaucoma," *Biomedical Signal Processing and Control*, vol. 24, pp. 34–46, 2016.

[19] J. R. H. Kumar et al., "Automatic optic cup segmentation using Kåsa's circle fitting technique," in *Proceedings of IEEE Region 10 Conference (TENCON)*, 2017, pp. 25–30.

[20] Liu et al, "Argali: an automatic cup-to-disc ratio measurement system for glaucoma detection and analysis framework," in *Medical Imaging 2009: Computer-Aided Diagnosis*, 2009, vol. 7260, p. 72603K.

[21] J. G. Zilly et al., "Boosting convolutional filters with entropy sampling for optic cup and disc image segmentation from fundus images," in *Proceedings of International Workshop on Machine Learning in Medical Imaging*, 2015, pp. 136–143.

[22] V. Pratt, "Direct least-squares fitting of algebraic surfaces," *ACM SIGGRAPH Computer Graphics*, vol. 21, no. 4, pp. 145–152, 1987.

[23] J. Sivaswamy et al., "Drishti-GS: Retinal image dataset for optic nerve head (ONH) segmentation," in *Proceedings of IEEE International Symposium on Biomedical Imaging (ISBI)*, 2014, pp. 53–56.

[24] E. Decenciére et al., "Feedback on a publicly distributed database: the Messidor database," *Image Analysis & Stereology*, vol. 33, no. 3, pp. 231–234, Aug. 2014.

Authorized licensed use limited to: Max-Planck-Institut fuer Informatik . Downloaded on November 15,2023 at 12:54:36 UTC from IEEE Xplore. Restrictions apply.